A NOVEL OF RECONFIGURABLE PLANAR ANTENNA ARRAY (RPAA) WITH BEAM STEERING CONTROL

M. T. Ali and M. N. M. Tan

Faculty of Electrical Engineering (FKE)
University of Technology Mara (UiTM)
Shah Alam, Selangor 40450, Malaysia

T. A. Rahman, M. R. Kamarudin, and M. F. Jamlos

Wireless Communication Center (WCC)
Universiti Teknologi Malaysia
UTM Skudai, Johor 81310, Malaysia

R. Sauleau

Institut d'Electronique et de Télécommunications de Rennes (IETR)
UMR CNRS 6164
University of Rennes 1
France

Abstract—A new antenna structure is formed by combining the concept of reconfigurable planar antenna array (RPAA) with the parasitic elements to produce beam steering patterns. The antenna has been integrated with the PIN diode switches that enable the beam to be steered in the desired direction. This has been done by changing the switch state to either *on* or *off* mode. In this work, a number of parasitic elements have been applied to the antenna, namely reflectors and directors. They are placed in between the driven elements, which is aimed to improve the beam steering angle. With such configuration, the main beam radiated by the array can be tilted due to the effect of mutual coupling between the driven elements and parasitic elements (reflectors and director). The unique property of this antenna design is that instead of fabricating all together in the same plane, the antenna's feeding network is separated from the antenna radiating elements (the patches) by an air gap distance. This allows reducing the spurious effects from the feeding line. The optimization results for the resonant

Corresponding author: M. T. Ali (mizi732002@yahoo.com).

frequencies of the antennas with variable air gap heights are also been studied. The antenna is made for 5.8 GHz. Good agreement is achieved between the simulation and measurement.

1. INTRODUCTION

The development of wireless communication has made a good impact on the field of the antenna design. When one considering adding new features to existing antennas, questions about the benefits and applications of doing so arise. Reconfigurable antenna will be an attractive feature in the modern wireless communication system because it enables to provide a single antenna to be used for multiple systems. In the reconfigurable antenna, the fundamental characteristics such as operating frequency, bandwidth, polarization characteristics and radiation pattern of the antenna can be changed by controlling switches such as PIN diode switches [1], field-effect transistor (FET) [2], photo conductor switches [3] or by electromechanical system (MEMS) switch [4]. By controlling the states of the switches, *on/off*, several approaches are proposed for implementing the reconfigurable antenna [5, 6].

The reconfigurable antennas have attracted much attention in wireless communication systems such as cellular-radio system, airplane radar, smart weapons protection and point-to-point propagation. One of the applications of the reconfigurable antenna is that it can desirably steer the beam pattern into many directions [7, 8]. The authors in [9]presented reconfigurable antennas, which have radiated in different beam patterns by adjusting the apertures and maintaining their operating frequencies. The antenna presented in [10] shows a dual band dipole antenna integrated with series MEMS switches. However, this method typically uses a dual operating frequency to reconfigure the beam pattern.

The design of microstrip antennas is strongly related to several characteristics, such as complexity, cost, sidelobe level and bandwidth. If array antenna and transmission lines are etched on the same layer, it has the advantage of lower manufacturing cost. Unfortunately, this combination increases the size of the antenna and at the same time will degrade the antenna performance. The degradation of this performance is due to two main factors. First, the transmission line will generate unwanted radiation which indirectly increases the sidelobe level and cross-polarization. Second, for reconfigurable antenna, the switches are inserted with antenna element to alter their fundamental characteristics. However, if these switches are fabricated on the same

plane, they will produce interference to the radiating element. In this paper, a new structure of planar antenna array constructed with separated feed line from the radiating elements by an air gap technique is proposed to overcome these problems.

This paper, the behaviors of Reconfigurable Planar Antenna Array (RPAA) with separated feeding lines have been studied and analyzed. Some of the feed line was removed at the back of the radiating element and mounted on a second substrate, separated from the radiating element by an interval (air gap technique). This technique allows reducing the unwanted spurious effects from the feeding line. The advantages of this design are that the radiation arising from the feeding line cannot interfere with the main radiation pattern generated by the antenna. This has been proven in Section 2.3. In this work, there are two antenna structures that have been studied and analyzed. The first antenna is a 16-element planar antenna array in which the feeding line is printed on the same plane as the radiating elements. Another antenna that has been constructed is a 16-element planar antenna array whose feed network is separated from the radiating elements by an air gap. Both antennas are designed at 5.8 GHz. In Section 3, the RPAA structures are integrated with and without parasitic elements. The simulated and measured results are presented to demonstrate the excellent performance of this antenna and to show that the steer beam deviation can be improved by parasitic elements.

2. STRUCTURE OF PLANAR ANTENNA ARRAY WITH SEPARATED FEED (PAASF)

This section describes the 4×4 planar array configuration comprises four sub-arrays arranged in a 2×2 configuration with separated feeding line by an air gap. Figure 1 shows the structure of the proposed antenna. The top antennas are fed by a vertical coaxial probe (SMA
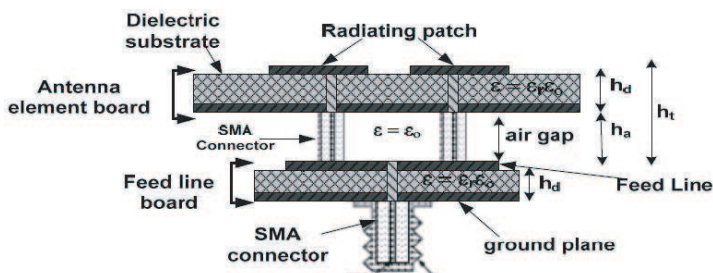

Figure 1. The schematic structure of PAASF with an air gap.

connector) that connecting the feed network to each sub-array. The air gap thickness (h_a) has been optimized to achieve a good return loss at 5.8 GHz. The unique property of this antenna design is that instead of fabricating all together in the same plane, the antenna's feeding network is separated from the antenna radiating elements (the patches) by an air gap distance. This allows to reduce spurious effects from the feeding line.

The configuration of PAASF will be investigated both simulatively and experimentally to obtain some quantitative guidelines for designing this type of antenna. The antenna designs are done with the basic structure of the proposed antenna, 2×2 planar array antenna (Sub-array) followed by the 4×2 planar array structure and finally full antenna structure, 4×4 planar array antenna with separated feeding network from the radiating elements by an air gap.
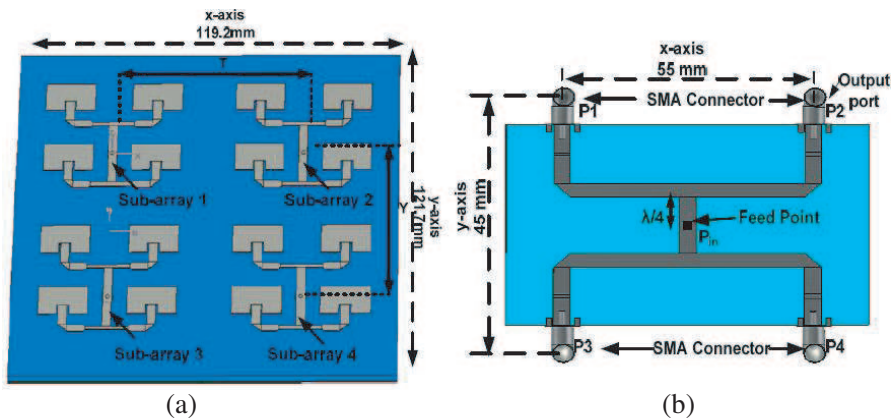
2.1. Antenna Structure

In this section, the driven element is used to radiate the transmission signal. It comprises a plurality of the sub-arrays (2×2 configuration patches) mounted along an x-axis and a y-axis on the substrate. Figure 2 shows the preferred structure of one of the sub-arrays. Each of the sub-arrays includes a plurality of radiating patches connected electrically by a transmission line. Various configurations are possible for the sub-arrays. However, in the preferred embodiment, each of the sub-arrays has at least four radiating patches arranged in pairs. The optimization of the various antenna dimensions will produce better performance, especially to determine the good return loss results. The
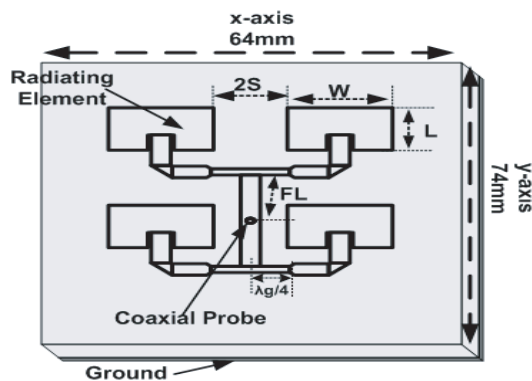

Figure 2. The schematic diagram of 2×2 structure array antenna (sub-array).

best performance of the return loss identified at -49 dB with the length of patch (L) is 11.3 mm. The width of patch (W) is 16.8 mm, and the feed line (FL) is 12 mm at 5.8 GHz.

Next, the 4×4 antenna element is constructed by comprising four sub-arrays on the single substrate with the size of 119.2×121.7 mm^2 as shown in Figure 3(a). The size of each patch is 16.8 mm $\times$ 11.3 mm, and their inter-element spacing is approximately $\lambda_o/2$. The spacing between the sub-arrays (T) along the x-axis direction is about 55 mm and along the y-axis (Y) direction 51.9 mm. The 4-way output (P1 to P4) power divider with single input (P_{in}) is used to connect all these sub-array as shown in Figure 3(b).

(a)   (b)

Figure 3. Schematic diagram of PAASF structure. (a) Antenna element. (b) Feeding line board.
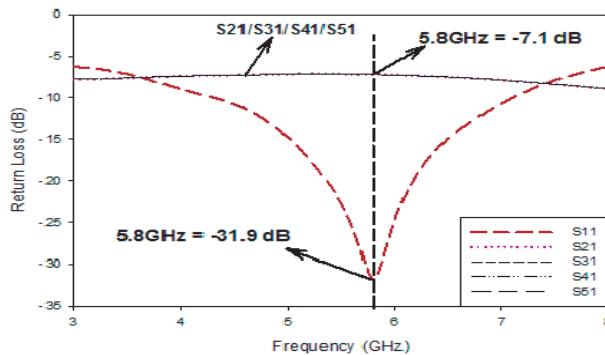
Figure 4. The simulated result of return loss for feed line board.

The feeding line structure is proposed as shown in Figure 3(b). Quarter wavelength transformers are used in the corporate feed network to maintain the input impedance at 50 Ohm. A coaxial probe is located at the center of the feed network as shown in Figure 3(b). The length of each transmission line is optimized before simulating the final structure. The simulated results of the feed line schematic diagram at 5.8 GHz using Applied Wave Research (AWR) software 2008 are given in Figure 4. The minimum simulated return loss is -31.9 dB at the operating frequency.

2.2. Air Gap Technique

The concept of constructed microstrip antenna with an air gap between the dielectric substrate and ground plane [11] is studied and shown in Figure 1. It is well known that using a thick and low permittivity substrate can increase the bandwidth of the microstrip antenna. The thickness of the microstrip antenna substrate will be increased by adding an air gap layer while keeping the average relative permittivity of the dielectric substrate of the antenna lower. Another advantage is the resonant frequency can be tuned by adjusting the air gap thickness without adjusting the antenna structure. This section presented a numerical study of the rectangular microstrip antenna with an air gap to calculate the resonant frequency with various air gap thicknesses. The calculated results based on the closed forms expression are compared with simulated results, and very good agreements are achieved. From the simulation, it is found that the resonant frequency can be tuned by optimizing the air gap thickness. The expression of the resonant frequency for the rectangular microstrip antenna with an air gap can be tuned by adjusting the air gap thickness and obtained as [11]:

$$f_r = f_{mn} = \frac{c_o}{2\sqrt{\varepsilon_{dyn}}} \sqrt{\left(\frac{m}{w_{eff}}\right)^2 + \left(\frac{n}{l_{eff}}\right)^2} \qquad (1)$$

where f_{mn} is the resonant frequency (f_r) in GHz, and subscript mn refers TM_{mn} modes. ε_{dyn} is the dynamic permittivity, and l_{eff} is the effective (electrical) length of the rectangular microstrip. w_{eff} is the effective (electrical) width of the rectangular microstrip in cm respectively, and c_o is the velocity of light in free space (300×10^6 m/s). This formula takes into account of the edge extension (fringing effect). To compute the resonant frequency of the dominant mode (TM_{01}), we make use of (1) by setting $m = 0$ and $n = 1$, thus

$$f_{mn} = f_{01} = \frac{15 \times 10^8}{l_{eff}\sqrt{\varepsilon_{dyn}}} \qquad (2)$$

The dynamic permittivity (ε_{dyn}) in (2) is a function of the dimensions, where the relative permittivity (ε_r) and the different modes field distribution are given by using an expression from [11].

$$\varepsilon_{dyn} = \frac{C_{dyn}(\varepsilon = \varepsilon_{av}\varepsilon_0)}{C_{dyn}(\varepsilon_0)} \tag{3}$$

An average relative permittivity (ε_{av}) is used to average the permittivity of the two-layer dielectric given by:

$$\varepsilon_{av} = \frac{\varepsilon_r h_d + \varepsilon_r h_a}{h_d + \varepsilon_r h_a} \tag{4}$$

where, ε_r is the relative permittivity of the dielectric substrate. h_a is the air gap thickness, and h_d is the dielectric substrate thickness. C_{dyn} $(\varepsilon = \varepsilon_{av}\varepsilon_o)$ and C_{dyn} (ε_o) in (3) are the total dynamic capacitance of the rectangular microstrip antenna with and without dielectric substrate $(\varepsilon_r = 1)$, respectively. These total capacitances can be obtained from [10], which we can simplify without loss of accuracy for TM$_{01}$.

$$C_{dyn}(\varepsilon_{av}\varepsilon_0) = \frac{\varepsilon_{av}\varepsilon_0 wl}{2h_t} + 2\left[\frac{1}{4}\left(\frac{\sqrt{\varepsilon_{eff}(w)}}{C_o Z(w, h_t, \varepsilon_r)} - \frac{\varepsilon_{av}\varepsilon_0 w}{h_t}\right)\right.$$
$$\left. + \frac{w}{2}\left(\frac{\sqrt{\varepsilon_{eff}(l)}}{C_o Z(l, h_t, \varepsilon_r)} - \frac{\varepsilon_{av}\varepsilon_0 l}{h_t}\right)\right] \tag{5}$$

The total dynamic capacitance of the rectangular microstrip antenna without dielectric substrate $(C_{dyn}(\varepsilon_o))$ can be determined by substituting $\varepsilon_{av} = 1$ into (5). Where $\varepsilon_{eff}(w)$ is the effective permittivity of the microstrip line, and $Z(w, ht, \varepsilon_{av})$ is the characteristic impedance of the microstrip line, which can be obtained as (6) and (7) respectively.

$$\varepsilon_{eff}(w) = \frac{\varepsilon_{av} + 1}{2} + \frac{\varepsilon_{av} - 1}{2}\left(1 + \frac{10h_t}{w}\right)^{-1} \tag{6}$$

$$Z(w, h_t, \varepsilon_r) = \frac{377}{\sqrt{\varepsilon_{eff}(w)}}\left[\frac{w}{h_t} + 1.393 + 0.667\ln\left(\frac{w}{h_t} + 1.444\right)\right]^{-1} \tag{7}$$

The $\varepsilon_{eff}(l)$ and $Z(l, h_t, \varepsilon_r)$ can be determined by using l instead of w in (6) and (7) respectively.

To compute the effective length of a rectangular patch in (2), the effect of the edge extension is taken into account because of the influence of fringing field at the edge of the radiating patch. The effective length can be obtained from [11] as:

$$l_{eff} = l + 0.5\left(\frac{\varepsilon_{eff}(w) + 0.3}{\varepsilon_{eff}(w) - 0.258}\right)\left(\frac{120\pi h_t}{z(w, h_t, \varepsilon_{av})\sqrt{\varepsilon_{eff}(w)}}\right) \tag{8}$$
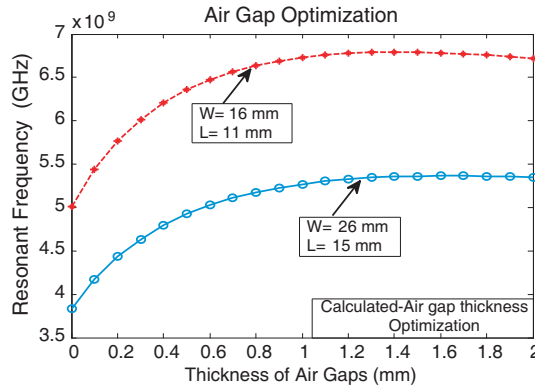
Figure 5. The calculated results of resonant frequency with variable an air gap thickness.

The calculated resonant frequencies of the single rectangular microstrip patch antenna with various air gap thicknesses are presented by using MATLAB software. The calculation of the resonant frequencies can be obtained by using Equation (2,) and the antennas were fabricated on the FR-4 substrate with dielectric constant, $\varepsilon_r = 4.7$, loss tangent, $\delta =0.019$ and substrate thickness, $h_d = 16$ mm. The calculated resonant frequency of the rectangular microstrip antennas with different air gap thicknesses (h_a) are shown in Figure 5. There are two sets of microstrip patch antennas were calculated with different dimensions of patch. The first antenna is calculated with the width and length of 16 mm and 11 mm, meanwhile the second antenna with the width and length of 26 mm and 15 mm, respectively. Both results illustrate that the resonant frequency increases while air gap thicknesses are increasing when such antennas have the same width and length.

Figure 6 shows that the resonant frequency increases with air gap thicknesses for simulated and numerical analysis. This simulated result was verified with the numerical results, in which the calculated resonant frequencies decrease while air gap thicknesses are increasing. It is apparent from the curve that increasing the air gap height induces a decrease of the resonant frequency. The best result providing a good impedance matching at 5.8 GHz is obtained at $h_a = 18.55$ mm with $S_{11} = -34.0$ dB. Hence, this height has been chosen in the final design. The simulated return loss and radiation pattern of the 4×4 rectangular microstrip planar array antennas with different air gap thicknesses (h_a) are shown in Figure 6(c).
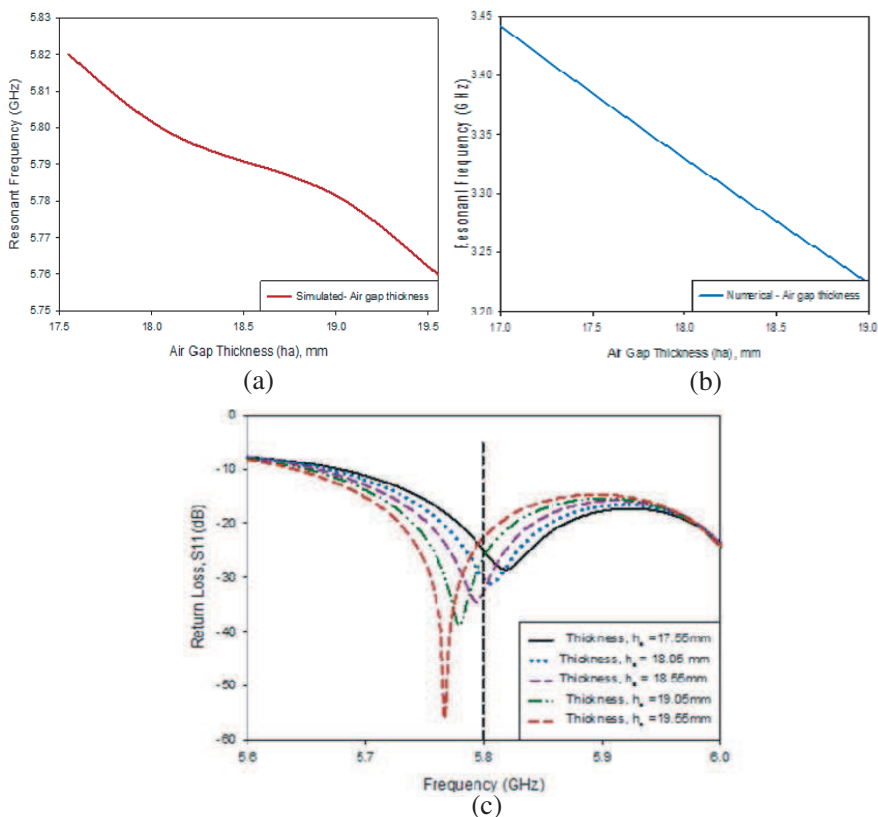
Figure 6. The result of resonant frequency with variable air gap thickness (h_a). (a) Simulated. (b) Numerical. (c) Return loss computed for different air gap heights.

2.3. Comparison of Planar Antenna Array with and without Air Gap (Separated Feed) Technique

In [12], the structure of planar antenna array between without ("Structure 1") and with ("Structure 2") an air gap was compared. The simulated observation has been done in terms of the size of the antenna, sidelobe level, antenna gain and return loss. All the comparison parameters are listed in Table 1. The comparison of simulated return loss for both structures, which have good impendence matching of $-29.4\,\mathrm{dB}$ and $-31.9\,\mathrm{dB}$, respectively. It is also noted from Figure 7(b) that the antenna gain generated by "Structure 2" of $11.8\,\mathrm{dB}$ is higher compared to $8.6\,\mathrm{dB}$ generated by "Structure 1". Since some of the transmission line is placed to another board, the
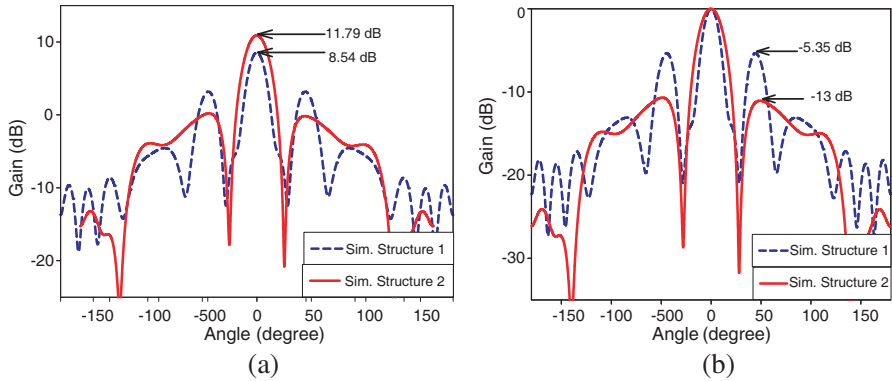
Figure 7. Comparison of simulated radiation pattern. (a) Non-normalized. (b) Normalized.

Table 1. The comparison simulated result between two structures.

Specifications	Structure 1	Structure 2
Antenna Gain (dB)	8.6	11.8
Side lobe to main lobe ratio (dB)	−5.4	−13.0
Antenna Size, $W \times L$ (mm^2)	179.8×185.0	119.2×121.7
Return Loss S_{11} (dB)	−29.4	−31.9

size of the antenna becomes smaller as shown in Table 1. Figure 7(a) presents a comparison of simulated radiation patterns for H-cut plane at 5.8 GHz. It can be seen that the magnitude of the side lobe level for "Structure 1" is clearly higher than that of "Structure 2", −5.4 dB and −13.0 dB respectively.

3. STRUCTURE OF RECONFIGURABLE PLANAR ANTENNA ARRAY (RPAA)

In this section, the Reconfigurable Planar Array Antenna (RPAA) is constructed by combining the PAASF with active feeding network. The RPAA is investigated to produce a scanning beam pattern. The beam diversity characteristic of the antenna was realized by controlling the switches mode on the feed line board. The switches were then used to select which port at the feed network were operative and supply the RF signal to antenna port for the purpose of changing the aperture's function during operation. The radiation characteristics for the designed antenna element and array antenna such as return
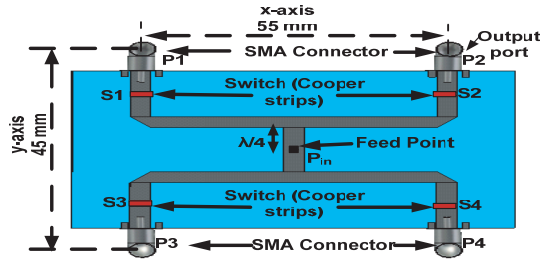
**Figure 8.** The feed line integrated with RF switching.

loss and H-plane radiation patterns were obtained by using Computer Simulation Technology (CST) Studio Suite 2008.

The integration of RF switches in PAASF was investigated to steer the beam by controlling the switches modes. To prove the concept in simulation, the switch is represented as a cooper strips. The integration of RF switches (used cooper strips to prove the concept, labeled S1, S2, S3, and S4 with red colour as in Figure 8) with the antenna elements will enable to tilt the beam pattern towards the desired direction. This can be done by controlling the switch modes to either *on* or *off* mode. When the switch is in the *off* state condition, the gap between feed lines occurs, no current flowing through the gap. There are three possibilities of configuration modes — Center Direction (CD), Right Direction (RD) and Left Direction (LD). The first configuration is to set the switches in *on*-mode for all the switches, CD. The second and third configurations require only two sets of switches, S1 and S3 (RD) or S2 and S4, (LD) in *off* mode conditions. For example, RD-mode means that the switches S1 and S3 are in *off*-mode, and the switches S2 and S4 are in *on*-mode. This means that the current will be distributed only from input port (Pin) towards port 2 (P2) and port 4 (P4) at antenna element. In this condition, only Sub-Array 2 and Sub-Array 4 will be generated. The signal and others elements act as passive elements. Table 2 tabulates the configuration of switching for RPAA.

To demonstrate the flexibility of the design approach, several cases have been presented to realize the scanning beam concept. The comparison of the simulated results of the return loss for all cases is demonstrated in Figure 9(a). The return losses of LD, CD, and RD modes are -21.5 dB, -34.5 dB, and -21.0 dB, respectively. The effect of switching contributes to the deflection of beam pattern direction by moving the beam toward right, left and center directions. According

Table 2. Antenna switching configurations.

Mode	Switch Configurations				Sub-array
	S1	S2	S3	S4	
CD	ON	ON	ON	ON	All sub-array active
RD	OFF	ON	OFF	ON	Sub-array 2 and 4 active
LD	ON	OFF	ON	OFF	Sub-array 1 and 3 active

(a)   (b)
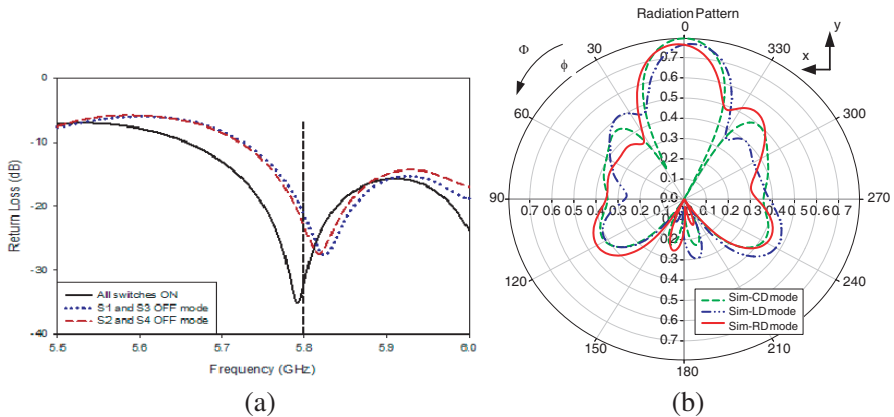
Figure 9. Simulated result of return loss and H-plane radiation pattern for different configurations at 5.8 GHz. (a) Return loss, S_{11}. (b) Radiation pattern — H-plane.

to the simulated results, the radiation pattern characteristic of the antenna forming has been tuned efficiently, and the pattern obtained is directed to three directions as shown in Figure 9(b). It is seen that by changing the mode of the switches, the beam can be steered in three directions. The simulated beam diversity angles were obtained at $-3.0°$, $0.0°$ and $+2.0°$, for LD, CD, and RD modes respectively, ("+" and "−" mean that the direction of the radiation pattern is steered towards the positive and negative x-axis, respectively). Only the simulated H-plane radiation patterns for resonant frequency are shown in Figure 9, while the E-plane patterns are omitted because they are always directed towards $0°$. The summarized simulated results of RPAA are shown in Table 3.

As a result, the structure of the antenna is not perfectly developed to produce large beam diversity angles. It is therefore assumed that this technique could be expanded to allow a large number of directions than described. However, good agreements can be observed from the

**Table 3.** The summarized simulated results of RPAA.

Switch Conf.	Gain (dB)	Sidelobe (dB)	Steering Angle	S_{11} at 5.8 GHz	HPBW
CD mode	11.8	−11.9	0.0°	−31.9	23.4°
RD mode	10.7	−9.0	+2.0°	−23.2	24.4°
LD mode	10.7	−10.5	−3.0°	−21.4	24.2°

results that the arrangement of the antenna structure is affected by a beam pattern. Another alternative approach for increasing the angle of steering beam is presented. The parasitic elements have been used in microstrip patch antennas in order to improve the angle of steering beam. The detailed concept of the RPAA with parasitic elements will be discussed in the next section.

3.1. Improved the RPAA with Parasitic Elements

A modified RPAA structure is formed by combining the concept of reconfigurable planar antenna array (as discussed in Section 2) with the parasitic elements technique to improve the angle of steering beam. The overall antenna structure is still the same as a previous antenna, using separated feed lines by an air gap technique as shown in Figure 1. The beam direction of the antenna can be improved due to the effect of mutual coupling and Yagi-Uda principle [13–15]. The Yagi-Uda concept is used in this antenna with parasitic reflector and director patches printed on the same plane of the driven element. The difference in this structure compared to the previous antenna is a number of parasitic elements which have been printed between the sub-array elements (reflector) and at two edges, right and left sides of the antenna (director).

A similar concept is presented in [16], to demonstrate the use of switched parasitic elements in electronic beam steering applications. Figure 10 shows that the antennas with parasitic elements have been used to steer the beam toward intended user. The antennas consist of three straight line rectangular microstrips printed in parallel on a grounded dielectric substrate. The driven element is placed at the center with parasitic strip elements on both sides, each with two switched connections. The configuration of this switch mode, *on/off*, will affect parasitic strips length, which can be lengthened or shortened with respect to the center strip. In this structure, the lengthened parasitic element acts as a reflector element, and the shortened parasitic element acts as a director element.
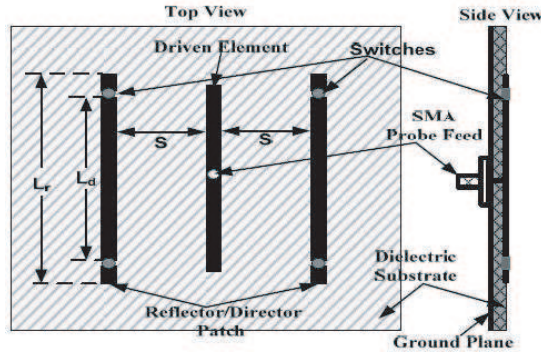
Figure 10. The geometrical structure of the RMPA [16].

Similar to the microstrip Yagi array antenna, the mutual coupling concept will be used in this antenna to control the radiation pattern. The induced currents on the parasitic element is generated because the mutual coupling has been affected by the direction of the beam. The lengthened parasitic element has bigger currents compared to driven element and shortened parasitic, such that it has much effect to tilt the beam toward the opposite direction with respect to broadside. When both parasitic elements shortening or lengthening that driven element, the antenna has a broadside radiation pattern. The optimized length of the reflector is 13% longer, and the director is 9% shorter than the driven element with spacing between them, approximately 20 mm.

The analysis of RMPA using transmission model illustrated in [16] indicates that the approach can provide pattern that can be configured without changes in the operating frequency. The current distribution on the antenna, including both phase and magnitude information, is required to calculate the angle of radiation pattern. The surface current on the patch induced by the magnetic field is given by;

$$\overline{J_s} = -\hat{z} \times \overline{H} = \hat{x} H_y - \hat{y}\, H_x \tag{9}$$

where

$$\overline{H} = \frac{j}{\omega \mu_o} \Delta \times \overline{E} = \hat{x} H_y + \hat{y} H_x$$

$$H_x = -\frac{j A_{mn}}{\omega \mu_o} \frac{n\pi}{W} \cos\left(\frac{m\pi x}{L}\right) \sin\left(\frac{n\pi x}{W}\right)$$

$$H_y = -\frac{j A_{mn}}{\omega \mu_o} \frac{n\pi}{L} \sin\left(\frac{m\pi x}{L}\right) \cos\left(\frac{n\pi x}{W}\right)$$

where A_{mn} is the coefficient of feed line.
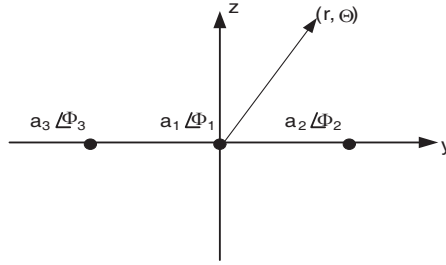
Figure 11. Radiation model of RMPA with relative's magnitudes and phases of currents on the elements.

The changed mutual coupling between closely spaced driven and parasitic elements by different spaces (s) results in effective distribution source current. Before calculating the radiation pattern, it is required to determine the current on the parasitic patches induced by the driving current. Therefore, the relationship between the ratio of the currents on two coupled patches and the ratio of the voltages on two ports is given as:

$$\frac{J_{xs'2}}{J_{xs'1}} \approx \frac{V_2}{V_1} = \frac{Z_{21}}{Z_{11}} \qquad (10)$$

And

$$\frac{J_{xs'3}}{J_{xs'1}} \approx \frac{V_3}{V_1} = \frac{Z_{31}}{Z_{11}} \qquad (11)$$

where $J_{xs'i} = a_i \exp\left(j\Phi_i\right)$, $i = \pm 1$, ± 2, and ± 3 is the current on patch i, with a_i the magnitude of current on patch, and Φ_i is the phase of current on patch. The radiation of a single current is isotropic in H-plane and will be identical to the array factor as shown in Figure 11.

$$F(\theta) = \sum_i J_{xs'i} \exp\left(-jkr_i\right), \ i = \pm 1, \ \pm 2, \ \text{and} \ \pm 3 \qquad (12)$$

where k is the phase constant in free space, and r_i is the distance from element I to the observation point. The radiation pattern in H-plane can be determined by substituting (10) and (11) into (12).

Figure 12 shows that the layout of antenna elements is printed with parasitic elements. With such a configuration, the main beam radiated by the array can be tilted due to the effect of mutual coupling between the driven elements and parasitic elements (director and reflectors). As seen in the Figure 12, four sub-array microstrip patches are etched together printed with parasitic elements on the same substrate with the size antenna of $109 \times 128\,\text{mm}^2$. It is smaller than the RPAA without parasitic because the spacing between two sub-arrays becomes narrow.
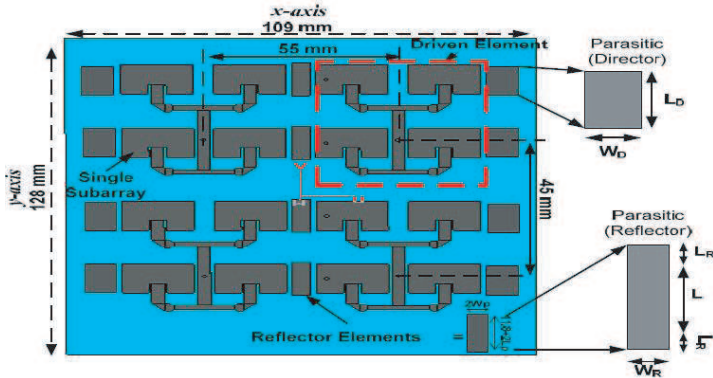
Figure 12. The structure of RFAA with parasitic element.
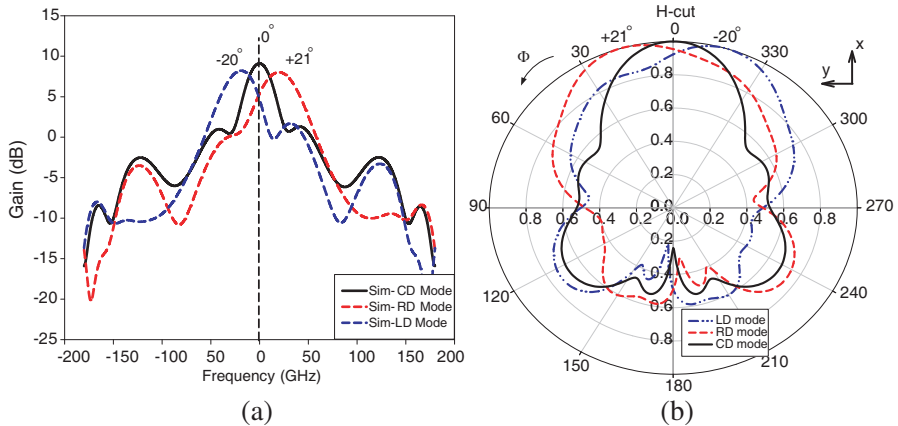
Figure 13. The simulated radiation pattern of RPAA with parasitic elements. (a) Rectangular plot. (b) Polar plot.

The size of the parasitics element (width (W_R) and length $(L + L_R)$ for the reflector and width (W_D) and length (L_D) for the director elements) is considered in parametric study to determine reasonable return loss at frequency 5.8 GHz. In the preferred embodiment, each of the parasitic reflector elements has a width (W_R) of 4 mm and a length $(L + L_R)$ of 13.3 mm. Each of the parasitic director elements preferably has a width (W_D) of 5 mm and a length (L_D) of 10.6 mm.

The beam diversity of the reconfigurable microstrip planar array antenna can be increased by adding parasitic elements and reducing spacing between the sub-arrays. Based on the simulated analysis, the optimum distance between the radiating patches and parasitic elements

for the largest steering beam is about 1.2 mm. The dimension ratio of
the parasitic element to the radiating patches ranges from 1.1 to 1.3.
When a parasitic element is added in the antenna structure, as shown in
Figure 12, the pattern shows improvements in terms of steering angle
compared to antenna without the parasitic elements. By using the
same schematic circuit of the switch diagram, the process of electrically
control (CD, LD and RD) in the feed line is similar to what was done
in Section 2. Figure 13 shows the simulated radiation pattern for the
RPAA when the switches in conditions *off*- and *on*-modes. It shows
that the angles of radiation pattern were steered to three directions,
+21°, 0° and −20°. Table 4 shows the simulated result of RPAA after
integrated with parasitic elements.

**Table 4.** The simulated results of RPAA with parasitic elements.

|	Switch Mode	Gain (dB)	Sidelobe (dB)	Steering Angle	S_{11} (dB)	HPBW (0°)
1	CD mode	8.7	−11.1	0.0°	−10.5	32.6°
2	RD mode	8.5	−11.7	$+21.0^\circ$	−21.9	39.0°
3	LD mode	8.6	−9.7	$−20.0^\circ$	−19.2	36.5°
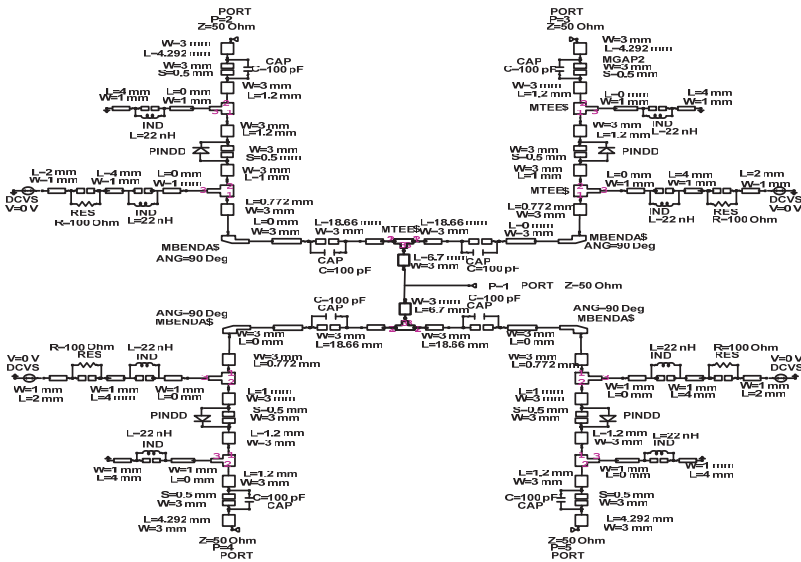
Figure 14. The equivalent circuit of feed network integrated with RF
switching circuit.

4. MEASUREMENT AND RESULT DISCUSSION

Figure 14 shows the schematic diagram of the switching circuit inserted in transmission lines. Each switching circuit consists of a PIN diode, two DC block capacitors, two inductors and one resistor. The capacitors, (C1–C2), are used as DC blocking, and the inductors, (L1–L2), are used as RF chokes which provide low impedance for dc. The biasing voltage (6 V or 0 V) has been connected to 100 Ω resistor to limit the current flow to the switch. The optimized parameters for the capacitance and inductance were chosen to be 6.8 pF and 22.0 nH, respectively. To validate the design procedures, AWR simulator is used for verifying the performance of the switching circuit. Figure 15 show the simulated results for the single schematic diagram of switching circuit when the switches in conditions *off* and *on*-modes. The PIN Diode switches are labeled as S1 to S4 as in Figure 16. When the
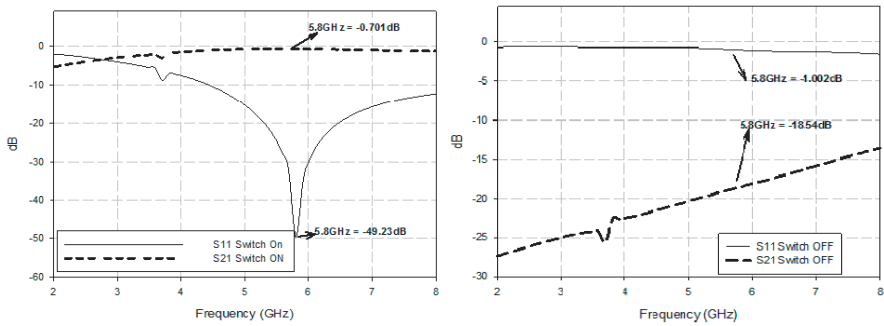
Figure 15. Calculated return loss (S_{11}) for ON and OFF states (a) switch ON mode and (b) switch OFF mode.
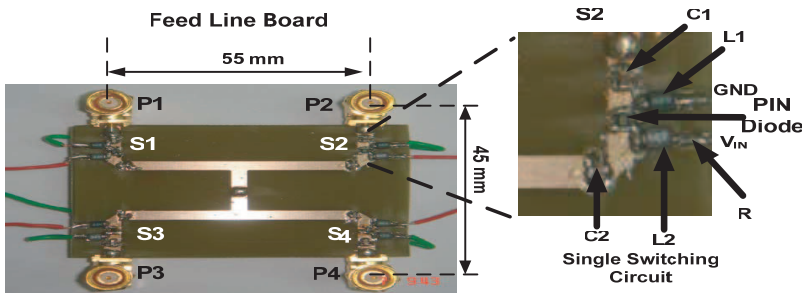
**Figure 16.** Prototype of feed line board printed with RF switches.
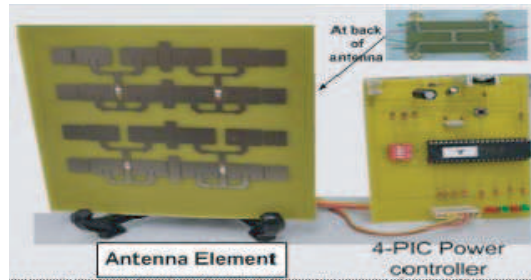
Figure 17. Prototype of RPAA with parasitic elements and 4-output PIC power controller.

Table 5. Comparison results of proposed antenna both with and without parasitic element.

Switch Conf.	Simulated		Measured	
	Angle	S_{11} (dB)	Angle	S_{11} (dB)
CD mode	$0.0°$	-10.5	$0.0°$	-17.4
RD mode	$+21.0°$	-21.9	$+17.0°$	-16.0
LD mode	$-20.0°$	-19.2	$-18.0°$	-18.0

switches are in the *off* state condition, a gap is created, hence, no current flows to the patches. The return loss (S_{11}) is obtained about -49.23 dB when the switch in *on*-mode and -1 dB when the switch in *off*-mode. The 4-output PIC power controller output is used to control and supply the DC voltage to activate the RF switches mode. The prototype of RPAA with 4-output PIC power controller is shown in Figure 17.

The normalized measured radiation patterns were plotted along with the simulated results at three states of switch configuration, which are CD, LD and RD modes. Figures 18 shows the radiation pattern produced by different *on/off* configurations of the switches. As predicted by the simulations, the radiation pattern behavior of the antenna remains nearly constant from one switch state to the next. There are three beam diversities; $0°$, $+17°$ and $-18°$ were obtained in the measurement and indicate that the beam diversity depends on the state of the switch operation. There is a slight decrease in maximum beam angle direction compared to the simulated results. Good agreement between the measurements and simulations has been obtained. The comparison of simulated and measured results of the beam diversity and return loss is listed in Table 5.
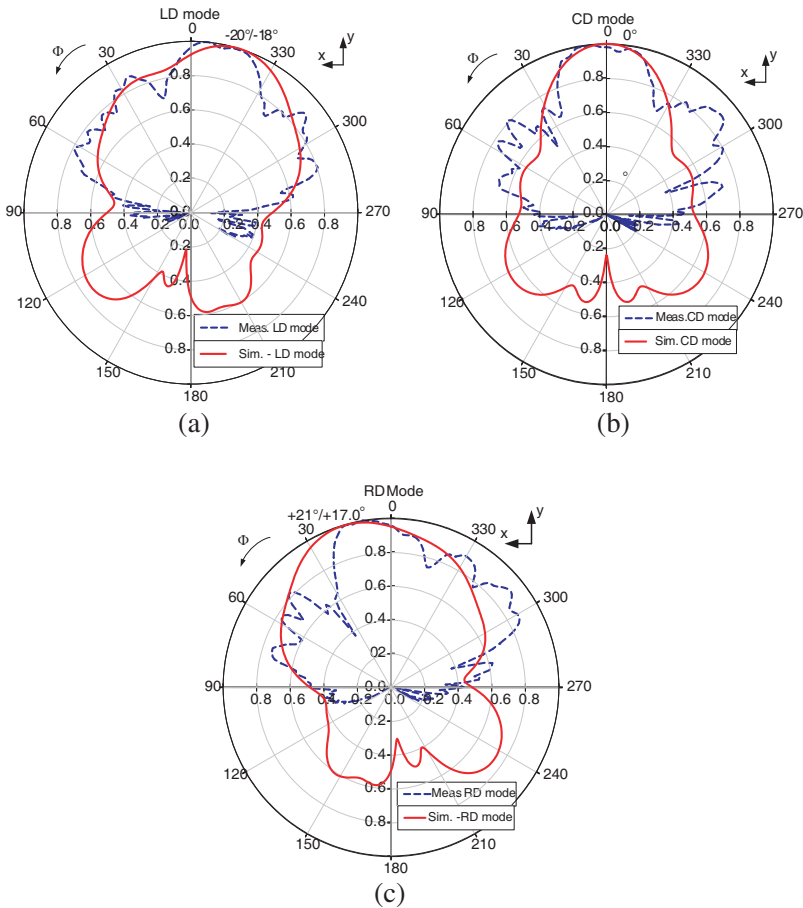
Figure 18. The measured results of radiation pattern at different switches configuration. (a) LD mode. (b) CD mode. (c) RD mode.

5. CONCLUSION

In this paper, simulated and measured data are demonstrated with the concepts of reconfigurable planar array antenna that produces steering beam pattern characteristic. The main objective of this work is to design and analyze the RPAA with its active feeding network (based on PIN diode switches) so as to steer the beam at resonant frequency, 5.8 GHz. The reconfigurable radiation beam antenna presented in this paper can be steered in three directions, $+17.0°$, $-0.0°$ and $-18.0°$, respectively at frequencies across the entire 5.8 GHz band, with

good transmission matching for all configuration modes. The antenna designs with various radiation patterns have great potential for wireless communication systems, such as point to point applications.

REFERENCES

1. Shynu, S. V., G. Augustin, C. K. Aanandan, P. Mohanan, and K. Vasudevan, "Design of compact reconfigurable dual frequency microstrip antennas using varactor diodes," *Progress In Electromagnetics Research*, PIER 60, 197–205, 2006.

2. Mak, A. C. K., C. R. Rowell, R. D. Murch, and C. L. Mak, "Reconfigurable multiband antenna designs for wireless communication devices," *IEEE Transactions on Antennas and Propagation*, Vol. 55, 1919–1928, 2007.

3. Panagamuwa, C. J., A. Chauraya, and J. C. Vardaxoglou, "Frequency and beam reconfigurable antenna using photoconducting switches," *IEEE Transactions on Antennas and Propagation*, Vol. 54, 449–454, 2006.

4. Cetiner, B. A., H. Jafarkhani, Q. Jiang-Yuan, Y. H. Jae, A. Grau, and F. de Flaviis, "Multifunctional reconfigurable MEMS integrated antennas for adaptive MIMO systems," *IEEE Communications Magazine*, Vol. 42, 62–70, 2004.

5. Wei, W.-B., Q.-Z. Liu, Y.-Z. Yin, and H.-J. Zhou, "Reconfigurable microstrip patch antenna with switchable polarization," *Progress In Electromagnetics Research*, PIER 75, 63–68, 2007.

6. Ali, M. T., M. R. B. Kamarudin, T. A. Rahman, R. Sauleau, and M. N. M. Tan, "Design of reconfigurable multiple elements microstrip rectangular linear array antenna," *Progress In Electromagnetics Research C*, Vol. 6, 21–35, 2009.

7. Kamarudin, M. R. B. and P. S. Hall, "Switched beam antenna array with parasitic elements," *Progress In Electromagnetics Research B*, Vol. 13, 187–201, 2009.

8. Chiao, J.-C., Y. Iao, I. M. Chio, M. Delisio, and L.-Y. Lin, "MEMS reconfigurable Vee antenna," *Digest of the 1999 IEEE MTT Intl. Microwave Symposium*, Vol. 4, 1515–1518, 1999.

9. Pringle, L. N., P. G. Friederich, S. P. Blalock, G. N. Kiesel, P. H. Harms, D. R. Denison, E. J. Kuster, T. L. Fountain, and G. S. Smith, "GTRI reconfigurable aperture design," *IEEE Antennas and Propagation Society International Symposium,* Vol. 1, 473–476, 2002.

10. Schaffner, J. H., R. Y. Loo, D. F. Sievenpiper, F. A. Dolezal, G. L. Tangonan, J. S. Colburn, J. J. Lynch, J. J. Lee,

S. W. Livingston, R. J. Broas, and M. Wu, "Reconfigurable aperture antennas using RF MEMS switches for multi-octave tunability and beam steering," *Antennas and Propagation Society International Symposium*, Vol. 1, 321–324, 2000.

11. Guha, D., "Resonant frequency of circular microstrip antennas with and without air gaps," *IEEE Transactions on Antennas and Propagation,* Vol. 49, 55–59, 2001.

12. Ali, M. T., T. B. A. Rahman, M. R. B. Kamarudin, M. N. M. Tan, and R. Sauleau, "A planar antenna array with separated feed line for higher gain and sidelobe reduction," *Progress In Electromagnetics Research C*, Vol. 8, 69–82, 2009.

13. Thiel, D. V., S. O'Keefe, and W. L. Jun, "Electronic beam steering in wire and patch antenna systems using switched parasitic elements," *Antennas and Propagation Society International Symposium, AP-S. Digest, 1996*, Vol. 1, 534–537, 1996.

14. Gray, D., L. J. Wei, and D. V. Thiel, "Electronically steerable Yagi-Uda microstrip patch antenna array," *IEEE Transactions on Antennas and Propagation*, Vol. 46, 605–608, 1998.

15. Mori, K., K. Uchida, and H. Arai, "Active antenna using parasitic elements," *IEEE Antennas and Propagation Society International Symposium*, Vol. 3, 1636–1639, 1998.

16. Zhang, S., G. H. Huff, J. Feng, and J. T. Bernhard, "A pattern reconfigurable microstrip parasitic array," *IEEE Transactions on Antennas and Propagation*, Vol. 52, 2773–2776, 2004.